Comparison of high resolution probe magnetics, X-ray fluorescence and permeability on core with borehole spectral gamma ray and spontaneous potential in an oil sand well

Toan H. To and *David K.* Potter*

Department of Physics, University of Alberta, Edmonton, Alberta, T6G 2E1, Canada

Abstract. The purpose of this study was to assess some novel techniques to improve oil sand reservoir characterization. The main focus was on high resolution, non-destructive, low field probe volume magnetic susceptibility measurements on slabbed core sections from an oil sands well in northern Alberta. The results demonstrated that this technique was able to distinguish the main lithologies (clean sands, inclined heterolithic stratification – IHS – beds comprising interbedded sand and clay, and shale) better than traditional borehole logging data such as gamma ray and spontaneous potential. The magnetic data also allowed estimates of a paramagnetic "illite" clay content parameter to be determined. High resolution X-ray fluorescence (XRF) measurements were taken at the same points as the magnetic susceptibility in order to provide supplementary elemental information. The magnetically derived illite contents correlated with the elemental contents of iron, potassium and aluminium (all components of illite) from the XRF. The magnetically derived illite contents also correlated with available fluid permeability measurements, and provided a tool for identifying anomalous mineralogies where the "illite" content exceeded 100%.

1 Introduction

This study primarily details the application of a novel, quantitative, high resolution probe magnetic technique for reservoir characterization of slabbed cores from an oil sands reservoir in Northern Alberta, Canada. The purpose was to produce an additional tool that complements, yet has significant advantages over, other traditional core and log based methods of oil sands reservoir characterization. Some preliminary work was previously reported [1, 2]. In the present study non-contact measurements of X-ray fluorescence (XRF) were also undertaken on the slabbed cores to support the interpretations provided by the magnetic technique. Reservoir characteristics and petrophysical properties are determined by various traditional methods using well logging, core analysis and well production data. Well logging allows in-situ estimation of properties, whereas core analysis allows ground trothing by performing measurements on recovered samples (rock and fluid) from the reservoir. Well production data gives generally large-scale information after a reservoir is in economic production. These traditional methods, however, have certain limitations. For example:

1. Borehole and laboratory core gamma ray techniques can be influenced not only by clay minerals (which often control permeability), but also by uranium in organic matter or small amounts of gamma ray emitting heavy minerals. Borehole gamma ray data can also be influenced by high gamma ray emitting drilling muds such as potassium chloride (KCl).
2. The spontaneous potential (SP) log is usually used to detect permeable beds based on the difference in salinity between the borehole fluids and the formation fluids, and causes a voltage deflection (generally measured in millivolts) from the shale baseline. However, if the salinities are equal there will be no deflection and the SP log will not be able to pick out the permeable zones in this situation.
3. Certain core analysis techniques are not always applicable in unconsolidated oil sands reservoirs. Often it is not possible to cut core plugs in such unconsolidated oil sands cores. In addition, some measurement techniques on slabbed cores might damage the cores. For example, standard probe permeability measurements require the probe tip to be sealed to the rock surface, and the procedure can lead to the probe tip puncturing and therefore damaging the core, resulting in incorrect permeability values. Other core measurement techniques, such as X-ray diffraction, can be time consuming, costly, and therefore tend to be limited to a small number (and small size) of samples.
4. For oil sands slabbed cores it is often difficult to visually recognize and quantify lithological changes in the cores when they are saturated with black heavy oil or bitumen. This paper will demonstrate how useful the probe magnetic method is in

* Corresponding author: dkpotter@ualberta.ca

identifying lithological changes and quantifying mineralogy in these situations.

5. Well production data can be useful for large scale interpretations, but not so useful for small scale high resolution lithological and sedimentological heterogeneities.

In contrast, the novel, quantitative probe magnetic technique and the XRF method used in this study are rapid and non-destructive. These techniques are particularly suitable for unconsolidated oil sands slabbed cores, unlike some other core analysis techniques that can potentially damage the cores as previously mentioned. Moreover, the probe magnetic sensor and recording meter are relatively inexpensive pieces of kit (totalling about $4,500 US for both items). The main applications of these techniques in this study were to identify the different lithologies and help quantify the mineralogy of the slabbed cores at high resolution, as additional tools to complement existing traditional methods. The oil sands well studied in this paper is located in the northeast region of the Athabasca oil sands near Fort McMurray. It was drilled to the McMurray Formation in the Mannville Group of the Western Canada Sedimentary Basin [3].

2 Core Screening Methods

2.1 Probe magnetic susceptibility

Magnetic susceptibility is usually expressed in terms of magnetic susceptibility per unit volume k as:

$$k = J/H \quad (1)$$

or in terms of magnetic susceptibility per unit mass χ as:

$$\chi = M/H = k/\rho \quad (2)$$

where J is the magnetization per unit volume and determined as the magnetic moment divided by the volume of the material, M is the magnetization per unit mass and determined as the magnetic moment divided by the mass of the material, H is the applied external magnetic field, and ρ is the density of the material. A Bartington MS2E sensor was used to perform high resolution measurements of magnetic susceptibility along the flat surface of the slabbed core. The sensor tip at the end of a ceramic tube (label **1** in **Figure 1 (A)** and label **4** in **Figure 1 (B)**) senses a rectangular surface area of 3.8 mm x 10.5 mm on the sample. This allows high resolution measurements to be made at the lamina scale. The sensor is calibrated to measure true volume magnetic susceptibility (k) when against a flat surface of a sample greater than 10 mm in thickness. Most of the magnetic susceptibility signal is acquired within a penetration depth of up to about 5 mm into the sample. The ceramic tube is mounted on a metal enclosure that houses the electronic circuitry. When the sensor is connected to the MS2 meter via a cable and the power is supplied, a low intensity alternating field (about 80 Am^{-1} and about 2 kHz in frequency) is generated. This applied field penetrates a few mm into the sample when the tip of the sensor is placed on the flat surface of the slabbed core. A calibration sample comprising magnetite particles dispersed in resin was used to check that sensor was working correctly.

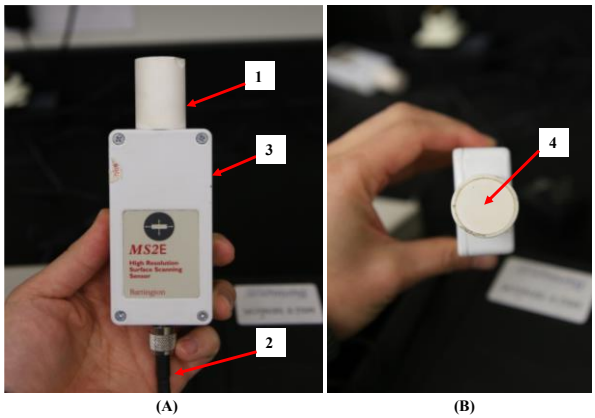

Fig. 1. MS2E probe sensor for surface magnetic susceptibility measurements on slabbed core. **(A)** side view showing: **1** is the probe tip with a ceramic guard and a sensor located at the end of the tube, **2** is the cable connected to the MS2 meter, **3** is a metal enclosure that houses the electronic circuity, and **(B)** top view **4** shows the cross section of the probe sensor tip that is gently applied to the surface of the slabbed cores.

Following the methodology in Potter et al [4] and Potter [5] each magnetic susceptibility value can be converted to an estimate of mineral content in simple model systems. Assuming that a rock sample is a two-component system of diamagnetic quartz and paramagnetic illite clay and that the contribution of fluids in the pore space in the sample is negligible (most reservoir fluids are diamagnetic [6] and will have little effect on the results), the proportion of each mineral component can then be estimated. The total measured magnetic susceptibility signal per unit volume is:

$$k_T = \{(F_I)\,(k_I)\} + \{(1-F_I)\,(k_Q)\} \quad (3)$$

where k_T is the total susceptibility value measured by the probe magnetic technique, F_I is the illite fraction per unit volume, $(1-F_I)$ is the quartz fraction per unit volume, and k_I and k_Q are the volume magnetic susceptibilities of illite (41×10^5 SI) and quartz (-1.64×10^5 SI), respectively. The illite fraction is then calculated as:

$$F_I = (k_T - k_Q) / (k_I - k_Q) \quad (4)$$

Note that from **Equation (4)** an illite content of around 4% or higher by volume in an illite + quartz mixture means that the net magnetic susceptibility signal of the sample is positive, whilst lower values mean the net signal is negative. Furthermore there are two key advantages of converting the raw magnetic susceptibility signal into a mineral content as follows:

1. The mineral contents can be plotted on logarithmic graphs (as long as the values are not zero), whereas raw negative magnetic susceptibility values cannot. This becomes important when correlating the magnetically derived illite content with other parameters such as fluid permeability.
2. Any values greater than 100% illite content using **Equation (4)** immediately indicate the presence of a mineral or minerals with higher positive magnetic susceptibility than illite.

2.2 X-ray fluorescence (XRF)

In an XRF measurement, two types of X-rays, Bremsstrahlung X-rays and characteristic X-rays, are involved. Bremsstrahlung X-rays are a continuous high energy spectrum generated by the X-ray source. These Bremsstrahlung X-rays eject electrons from the inner shells of atoms. Then, the vacancies left by the ejected electrons are quickly filled by other electrons dropping down from the outer shells as the atoms attempt to regain stability. During this latter process characteristic X-rays are emitted and received by the analyzer, and their precise energies are associated with the difference between the energy levels of the outer and inner electron shells of the atom. Since the distance between electron shells is different for each element, the energy level of each electron shell and the difference in energy between the shells are also different for each element. The emission of characteristic X-rays is the foundation of an X-ray fluorescence analysis.

In this study elemental contents in the slabbed cores of the oil sands well were quantified by the application of a portable XRF analyzer, the Thermo Scientific Niton XL3t [7], supplied by Elemental Control Limited (Toronto). The analyzer is designed to work either in a laboratory or as a field operation device. The analyser can be positioned in a customized stand for accurate portable, non-destructive measurements in the laboratory or used as a handheld device in the field. The analyzer contains an X-ray tube that emits radiation only when the shutter is opened, and a detector to detect the characteristic X-rays of the elements in a sample. The radiation of the Bremsstrahlung X-rays is produced by the analyzer and emitted through the measurement window, and the radiation of the characteristic X-rays, which is generated by ejected electrons, also reaches the detector through the window. Therefore, during a measurement the sample should always be in contact with the window.

For sedimentary rock samples, as in this study, the analyzer was used in “Mining Cu/Zn mode” as recommended in the manual [7]. It was calibrated with a reference sample with known values for Fe and K. The instrument operates with four different filters in order to obtain accurate results for a wide range of elements. Each measurement takes a total of 3 minutes, with 45 seconds for each filter beam. In the laboratory, the cores are usually measured in the form of pressed powder, or are cut into small pieces for use with suitable portable stands. However, to measure the slabbed cores in the present study, the device needed to be kept in contact with the surface of the cores during the measurements. The measurement time was too long for one to hold the device by hand during the operation, so we fabricated a customized stand to ensure the accuracy of the results (**Figure 2**). The stand was simply comprised of two legs and a bridge that allowed the height of the analyzer to be suitably adjusted in relation to the surface of the slabbed cores. With the support of the stand, the analyzer was always stable, and therefore the measuring window was always in contact with the surface of the slabbed cores during the measurements. Each XRF measurement analyzes a small area of 3 mm in diameter on the slabbed core, and a depth of penetration up to a few millimetres (very similar to the magnetic susceptibility probe). The XRF readings were taken in the middle of each corresponding area previously analysed by the magnetic susceptibility probe. The analyzer was connected to a PC with an application that allowed one to control the XRF measurement from a safe distance. This helped to minimize the dose of radiation received by the operator during the measurements.

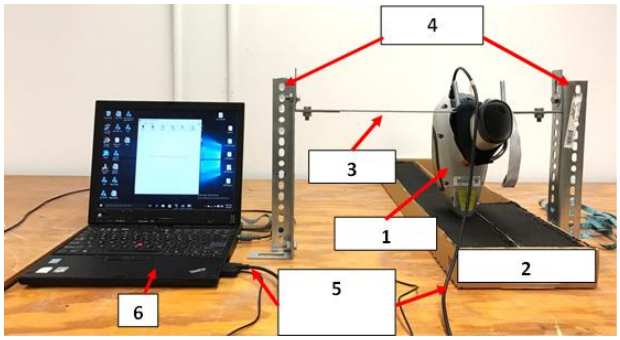

Fig. 2. The set-up for XRF measurements on the oil sands slabbed cores. **1** is the XRF analyzer, **2** is the slabbed core, **3** is the bridge of the stand, **4** shows the legs of the stand, **5** is the cable connecting the analyzer and the computer, and **6** is the laptop computer with an application to control the XRF analyzer from a distance.

3 Results and discussion

3.1 Probe magnetic susceptibility on slabbed oil sands core: example illustrating a key advantage of this technique

Figure 3 shows the probe volume magnetic susceptibility profile for a short oil sands slabbed core section saturated with bitumen in the well. Since quartz sand is diamagnetic and bitumen is also expected to be diamagnetic then it’s not surprising that all the data points in this example exhibit negative magnetic susceptibility. The probe results show real quantitative variations greater than the measurement uncertainties shown. A major advantage of the quantitative probe magnetic measurements is that they reveal variations that one cannot see from mere visual observations, since the black bitumen obscures any small differences in the mineralogy.

There are a number of possible reasons for the variations in magnetic susceptibility in **Figure 3**. The most likely explanation is due to the presence of small amounts of paramagnetic clay mixed with the sand. Another possibility is the presence of a very small amount of ferrimagnetic particles (such as magnetite). A further possible reason could be slight variations in the porosity and the bitumen saturation within the pore space. The MS2E sensor probe volume magnetic susceptibility measurements are susceptible to variations in porosity (though the effect is likely to be very small).

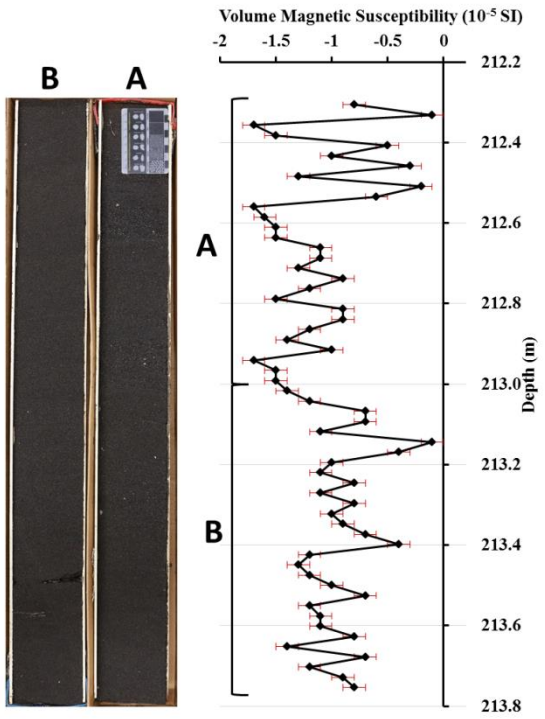

Fig. 3. Typical results of the MS2E probe volume magnetic susceptibilities measured on a short 1.6 m section of oil sands slabbed core saturated with black bitumen in the well. The magnetic probe is able to identify quantitative variations in the core that are extremely difficult to determine from mere visual observations. Uncertainty bars are shown.

3.2 Comparison of probe magnetic results with downhole log data

Figure 4 shows the depth profiles of probe volume magnetic susceptibility on the slabbed core, downhole total gamma ray (GR), and spectral downhole GR in a 68 m interval. **Figure 4** (left hand plot) clearly shows how the probe volume magnetic susceptibility measurements (far left curve) can differentiate the 3 main lithology types in this well. At the top of the profile (depths 149.4–159.1 m) the magnetic susceptibility values are highest and positive, indicating shale. In the middle of the profile (depths 161.7–183.0 m) the magnetic susceptibility values are generally positive and relatively low, which generally means some clay mixed with sand in these oils sands wells, and in this case represents the inclined heterolithic stratification (IHS) beds. At the bottom of the profile (depths 184.9–216.4 m) the magnetic susceptibility is generally negative, indicating clean sand (diamagnetic quartz), which is the best oil sands reservoir interval.

The total GR curve (right hand curve in the left hand plot of **Figure 4**) generally follows the trend of the magnetic susceptibility profile (high GR in the shale, lower GR in the clean sand), however the GR does not distinguish the different lithologies quite as well as the magnetic susceptibility. For example, between depths 162–168 m the total GR signal decreases, suggesting that this may be a clean sand interval. However, the positive magnetic susceptibility values suggest this is actually part of the interbedded clay and sand IHS beds. The spectral gamma ray signals (right hand plot of **Figure 4**) indicate that the total gamma ray signal is influenced by the thorium content, which drops significantly in the 162–168 m interval. It is not clear at present why the thorium content is lower in this interval. Several lines of evidence support the interpretation of IHS beds from the magnetic susceptibility:

(i) The magnetically derived illite content (far left curve of the left plot in **Figure 5**) shows values of 3–15% in this interval, which is more consistent with the IHS beds. Moreover, the spectral potassium gamma ray (**Figure 4**) follows the trend of the magnetically derived illite content (**Figure 5**). Potassium is a component of illite, and the spectral potassium curve shows no significant decrease in the interval 162–168 m, consistent with this interval being part of the IHS beds.

(ii) The grain size profile (right hand plot of **Figure 5**) clearly illustrates the three main lithologies (shale, IHS beds with interbedded clay and sand, and coarser grained clean sand), which correspond to those in the magnetic susceptibility (**Figure 4**) or magnetically derived illite (**Figure 5**) profiles. In particular, the grain size profile clearly shows the IHS beds extending from 161.7 to 182.2 m and containing a number of thin layers of very fine sands interbedded with thin layers of clay, and not clean sand in the interval 162–168 m as suggested by the total GR.

(iii) The deflection of the spontaneous potential (SP) curve in this interval (right hand curve of the left plot of **Figure 5**) is not larger than in the rest of the IHS bed interval, again supporting the interpretation from the magnetic susceptibility that the 162–168 m interval is part of the IHS beds with higher clay content and lower permeability than the clean sands below depth 184.9 m.

The total GR curve in **Figure 4** is also very variable and quite high in parts of the "clean sand" interval. The magnetic susceptibility is very low (mainly negative values due to diamagnetic quartz) and so picks out the clean sand much more clearly. If one used the total GR log data alone it would be much more difficult to be sure this was a large clean sand interval and one might misinterpret part of this interval as interbedded clay and sand.

The magnetic results clearly pick out a thin bed of an anomalous mineral or minerals with a high magnetic susceptibility (**Figure 4**) corresponding to a magnetically derived illite content greater than 100% (from the simple quartz + illite mixture model of **Equation (4)**) at a depth of about 158 m (**Figure 5**). The total GR, spectral GR and SP curves don't pick out this thin bed as clearly as the magnetic data does, even though the magnetic data is averaged over the same vertical interval as each wireline log data point averages.

Comparisons between the magnetically derived illite contents and the SP log (**Figure 5**) show correspondences in the two profiles with depth. In particular, one of the lowest illite contents occurs at exactly the same depth (in the clean sand) as the largest deflection of the SP log to the left, both curves suggesting a permeable zone at this depth.

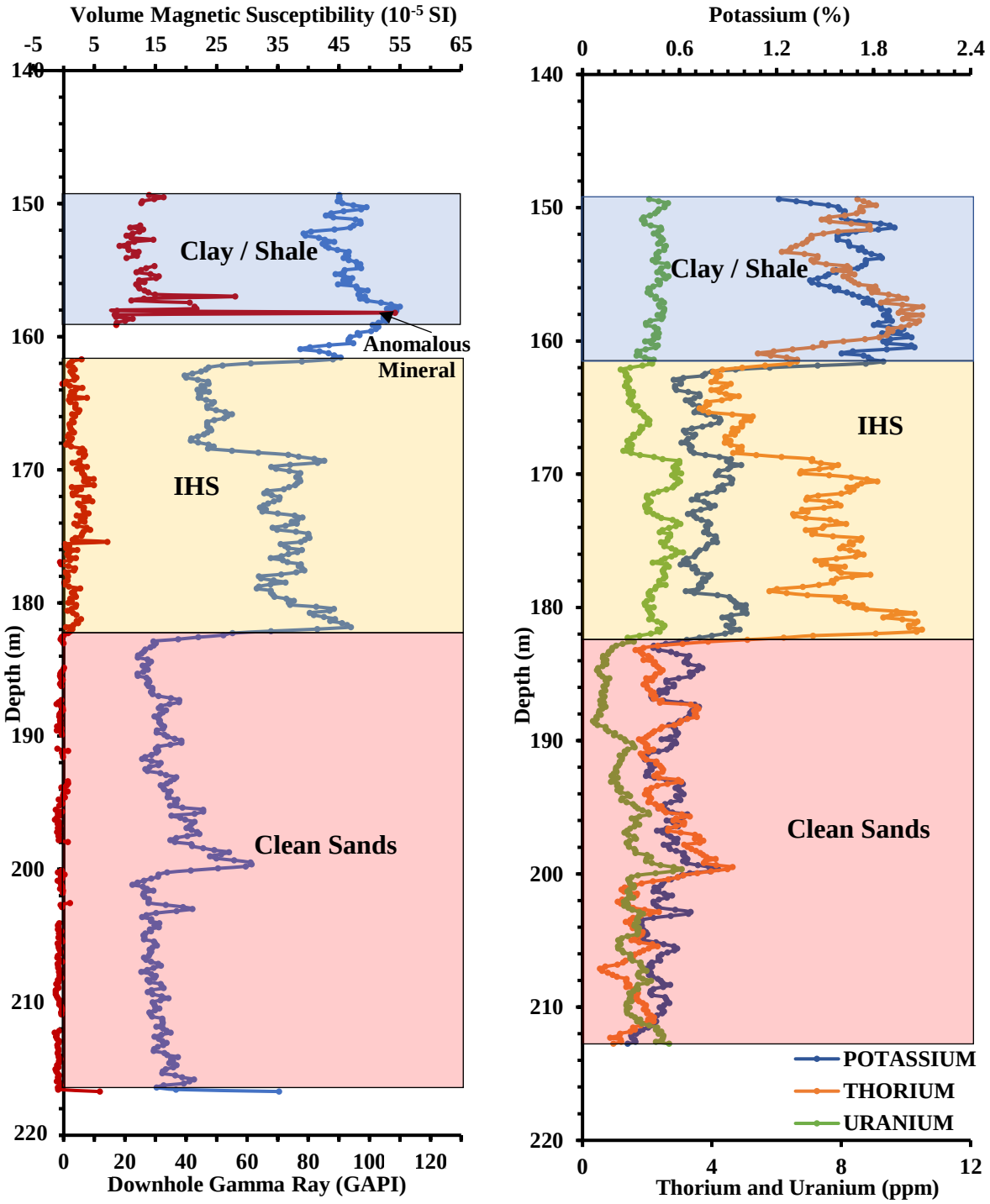

Fig. 4. Comparisons between the magnetic susceptibility results and the downhole gamma ray logs. **Left:** comparison of the vertically averaged, every 0.3048 m (1 ft), probe volume magnetic susceptibility (far left curve) and the total gamma ray log (right curve). **Right:** the spectral gamma ray logs of potassium, thorium and uranium.

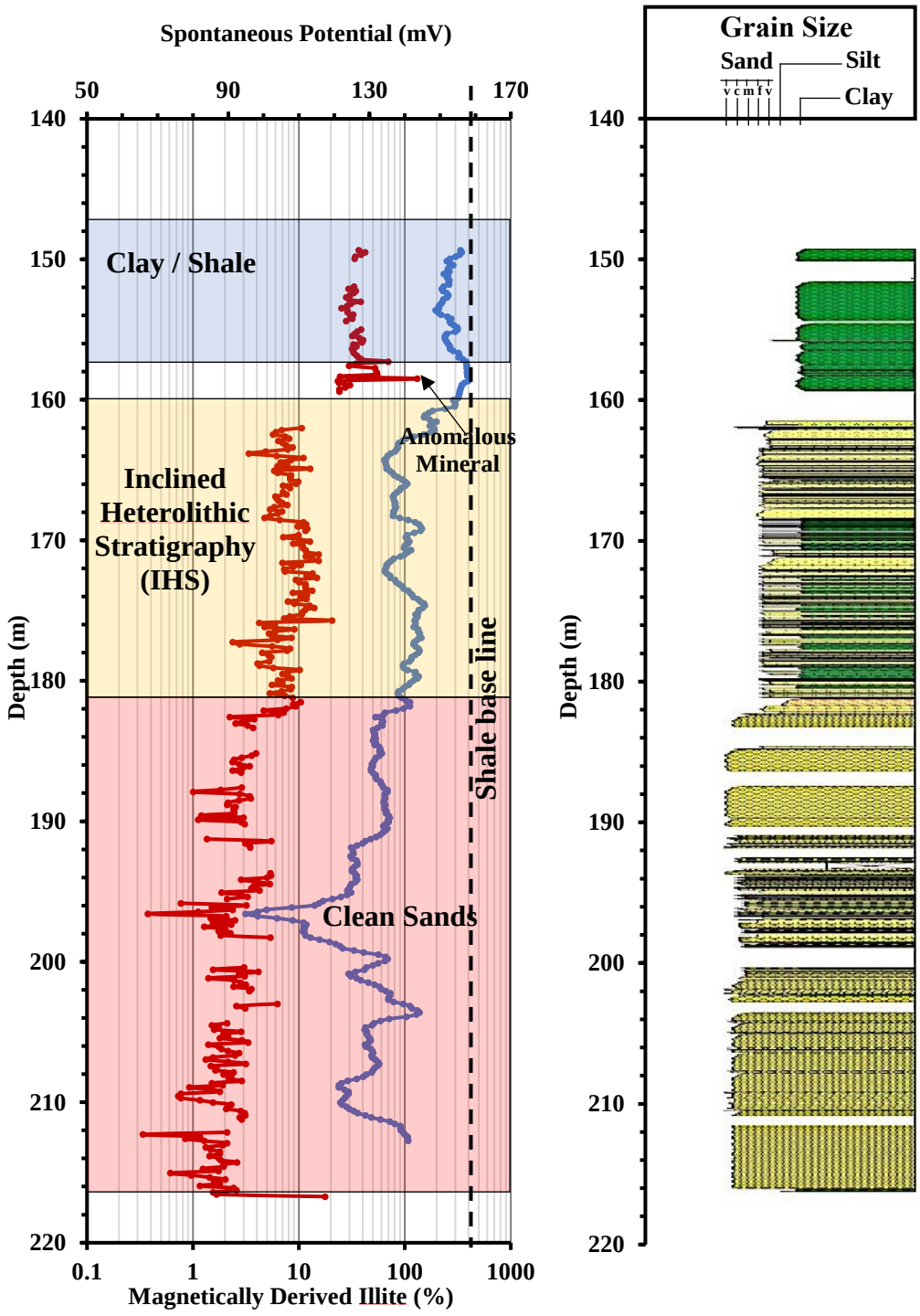

Fig. 5. Left: comparison of the vertically averaged, every 0.3048 m (1 ft), magnetically derived illite contents by volume (far left curve) and the SP log (right curve). **Right:** the grain size profile, which was determined from the slabbed core manually and displayed using Applecore™ software.

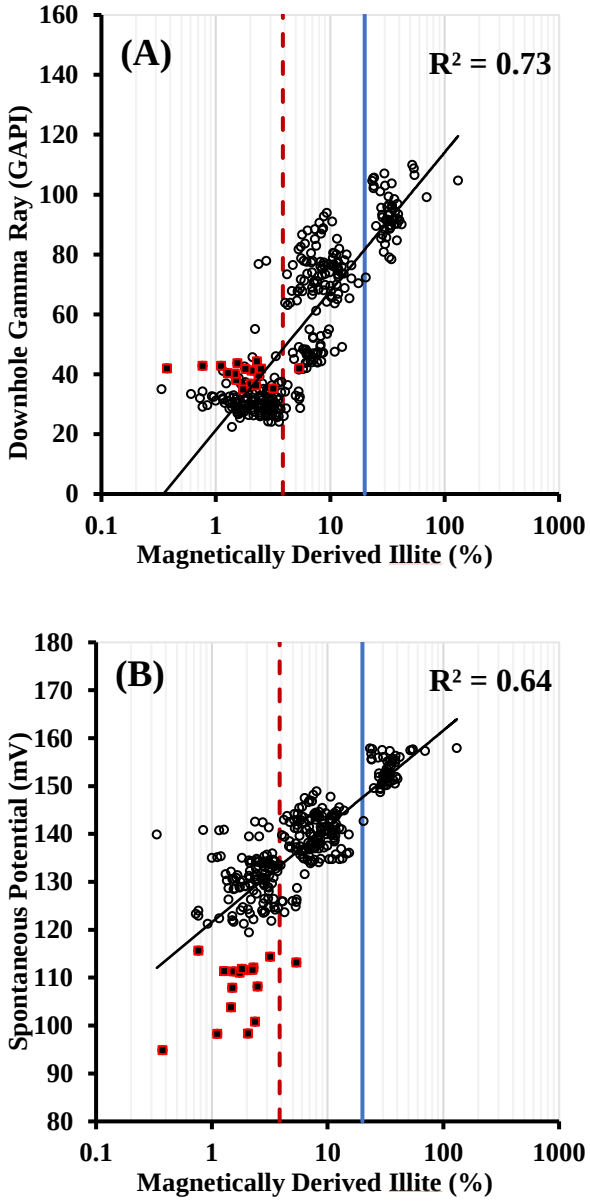

Fig. 6. Crossplots of the vertically averaged, every 0.3048 m (1 ft), magnetically derived illite contents by volume and the **(A)** total gamma ray log data, and **(B)** spontaneous potential log data. The dashed vertical line represents 3.85% illite, whilst the solid vertical line represents 20% illite.

3.2 Correlations between magnetically derived illite content, downhole log data and permeability

Figure 6 shows crossplots of magnetically derived illite contents using **Equation (4)** and the total GR and SP log data, with correlation coefficients of R^2 = 0.73 and 0.64. The coefficients increase to 0.75 and 0.69 if one omits the square data points, which correspond to the largest deflection of the SP curve to the left (lowest SP values), and some of the lowest illite contents. **Figure 6** shows that the crossplots have 3 clusters relating to the clean sand, the IHS beds, and the clay/shale. The dashed vertical line at 3.85% and solid line at 20% differentiate the 3 clusters. In general the clean sand is below 3.85% illite, the IHS beds between 3.85 and 20% illite, and the clay/shale greater than 20% illite.

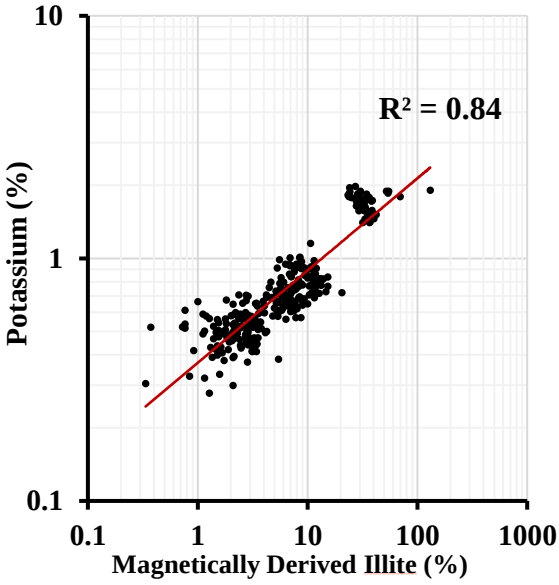

Fig. 7. Crossplot of the vertically averaged, every 0.3048 m (1 ft), magnetically derived illite contents by volume with the spectral potassium downhole gamma ray log data.

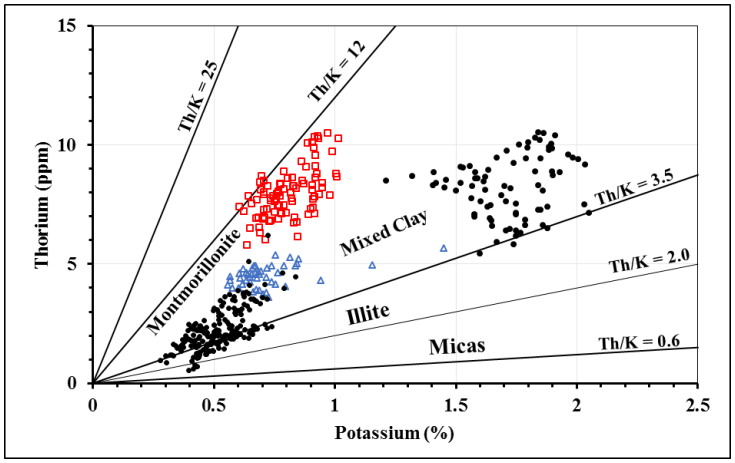

Fig. 8. Spectral gamma ray potassium versus thorium crossplot for this well (plotted on a standard Schlumberger chart CP-19). Upper right solid symbol cluster (19.7% of data points) is shale, and lower left solid symbol cluster (48.2%) is relatively "clean" sand. Open triangle cluster (10.8%) is IHS beds in the interval 161.7-168.4 m. Open square cluster (21.3%) is IHS beds in the interval 168.4-182.2 m.

Figure 7 shows a crossplot of the magnetically derived illite contents against the spectral potassium gamma ray log data. The high regression coefficient R^2 = 0.80 is consistent with illite being a key clay mineral in these oil sands. Our simple 2 component quartz + illite model from **Equations (3)** and **(4)** assumes that the "illite" includes mixed paramagnetic clays and micas, since "illite" is the only positive magnetic susceptibility component in the equations. Our "illite" content is effectively a catch all "magnetically equivalent illite" parameter and is useful because it correlates with several other key parameters as we show in this paper. The other

mixed clays in general have a range of magnetic susceptibility values quite close to that of illite. The spectral GR log data in **Figure 8** shows that virtually all the data points are within the illite, mixed clay and mica regions. Note that the data in **Figure 8** needs to be treated with some caution, however, since the points can be affected by other minerals present in the samples (e.g., small amounts of gamma ray emitting heavy minerals can shift the points to higher potassium and thorium contents).

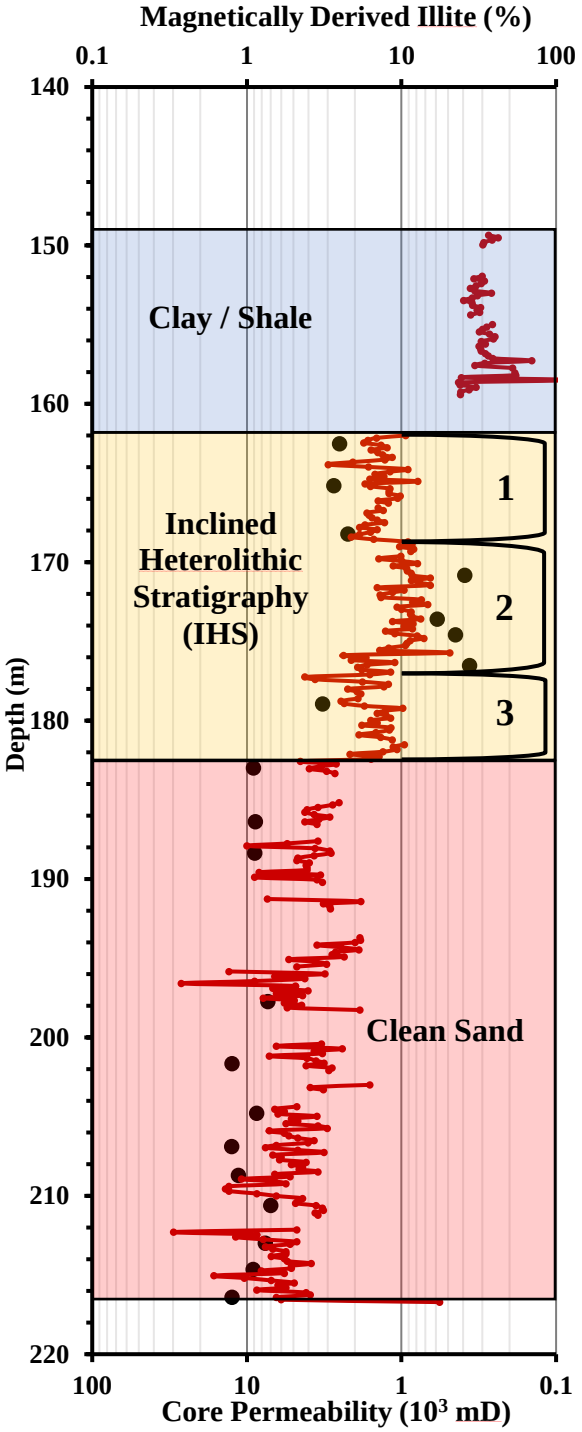

Fig. 9. Profiles with depth comparing the core permeability values (black circles) with the depth-matched magnetically derived illite contents by volume (curve).

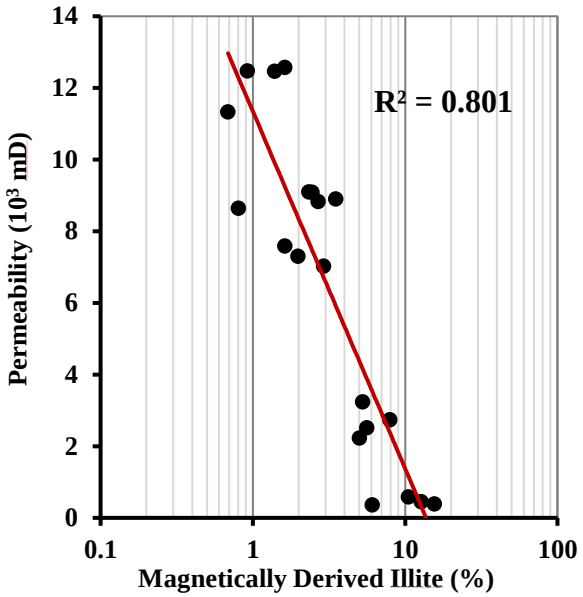

Fig. 10. Crossplot between the core permeability values and the depth-matched magnetically derived illite contents by volume.

Around 20 core air permeability measurements were available between the depths of 162–216 m. **Figure 9** shows the comparisons between the core permeability values and the magnetically derived illite contents with depth. The core permeability results correlate very well with the trend of magnetically derived illite content, but to a lesser extent with the SP curve (**Figure 5**). In the clean sand interval (185–216 m), the high permeability values (from 7.0 x 10^3 mD to 12.5 x 10^3 mD) correlate with low illite contents (generally less than 4%) and larger deflections to the left of the SP curve. In the IHS beds (161.7–183 m) the lower permeability values (from 0.4 x 10^3 mD to 3.2 x 10^3 mD) correlate with higher illite contents and less of a deflection to the left of the SP curve. However, the magnetically derived illite contents appear to correlate with the core permeability values better than the SP log in these IHS beds. Interval 2 in the IHS beds (**Figure 9**) has the lowest core permeability values which correlate with higher magnetically derived illite contents, while higher core permeabilities in intervals 1 and 3 (**Figure 9**) correlate with lower magnetically derived illite contents. In contrast, the variation of the SP log (**Figure 5**) does not clearly show the differences in permeability between these intervals.

Figure 10 shows a crossplot of the measured core permeability data with the depth-matched magnetically derived illite contents. The plot clearly indicates a strong relationship (R^2 = 0.801) between the core permeabilities and the magnetically estimated illite contents. A crossplot between the core permeability and the corresponding depth-matched SP log data (not shown) gives a much lower correlation (R^2 = 0.42), supporting our suggestion above that the trend of the magnetically derived illite contents better matches the trend of the core permeability values.

3.3 Correlations between magnetically derived illite contents and elemental contents from X-ray fluorescence

The crossplots of **Figures 11, 12** and **13** clearly show increasing Fe, Al, and K contents with higher magnetically derived illite contents, consistent with these elements being components of illite. The R^2 regression coefficient is 0.62 between the magnetically derived illite contents and both Fe and Al elemental contents, but a bit lower at 0.45 between the magnetic results and K content. In contrast, a crossplot (not shown) between magnetically derived illite contents and Ca contents showed no correlation (R^2 = 0.03) as expected as there were virtually no carbonates in the interval studied.

The crossplots also show clusters of data points which represent different lithologies. The clay / shale region is distinguished from the other lithologies with generally more than 20% magnetically derived illite content by volume and 2-7%, 1-2%, and 3-7% of Fe, K and Al respectively. In these crossplots the clean sand and IHS bed data tends to merge into one large cluster, although in general the clean sand has <4% magnetically derived illite content and <0.5%, <1% (most <0.6%) and <1% of Fe, K and Al respectively, whereas the IHS beds generally have around 4-20% magnetically derived illite content and 0.1–1% (mainly above 0.2%) Fe, 0.2–1% K and 0.5–3% Al.

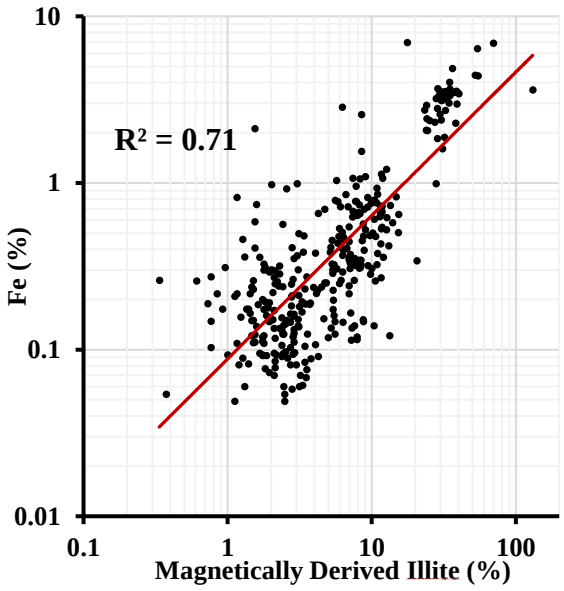

Fig. 11. Crossplot of the magnetically derived illite contents by volume against the Fe contents measured by the XRF technique on the slabbed cores.

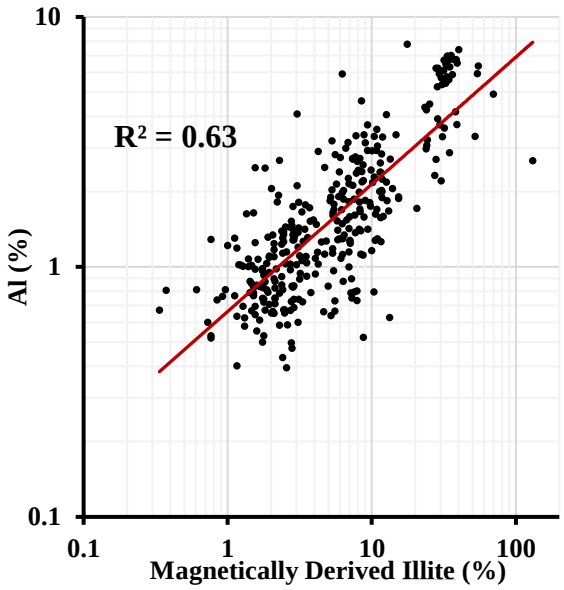

Fig. 12. Crossplot of the magnetically derived illite contents by volume against the Al contents measured by the XRF technique on the slabbed cores.

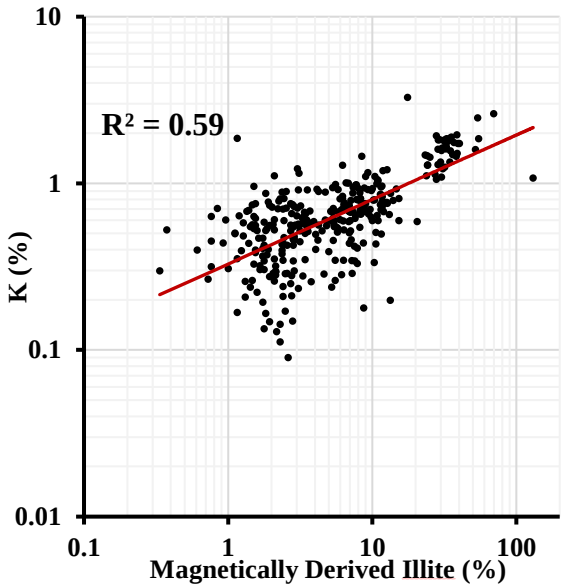

Fig.13. Crossplot of the magnetically derived illite contents by volume against the K contents measured by the XRF technique on the slabbed cores.

The profiles with depth of the elemental contents from the XRF measurements for Fe and K (**Figure 14**) and Al (**Figure 15**) show correspondences with the magnetic susceptibility (**Figure 4**) and the magnetically derived illite contents (**Figure 5** and the right hand curve in the right plot of **Figure 14**). This is consistent with these 3 elements all being components of illite. All 3 elements significantly increase in the more clay rich shale interval at the top of the section.

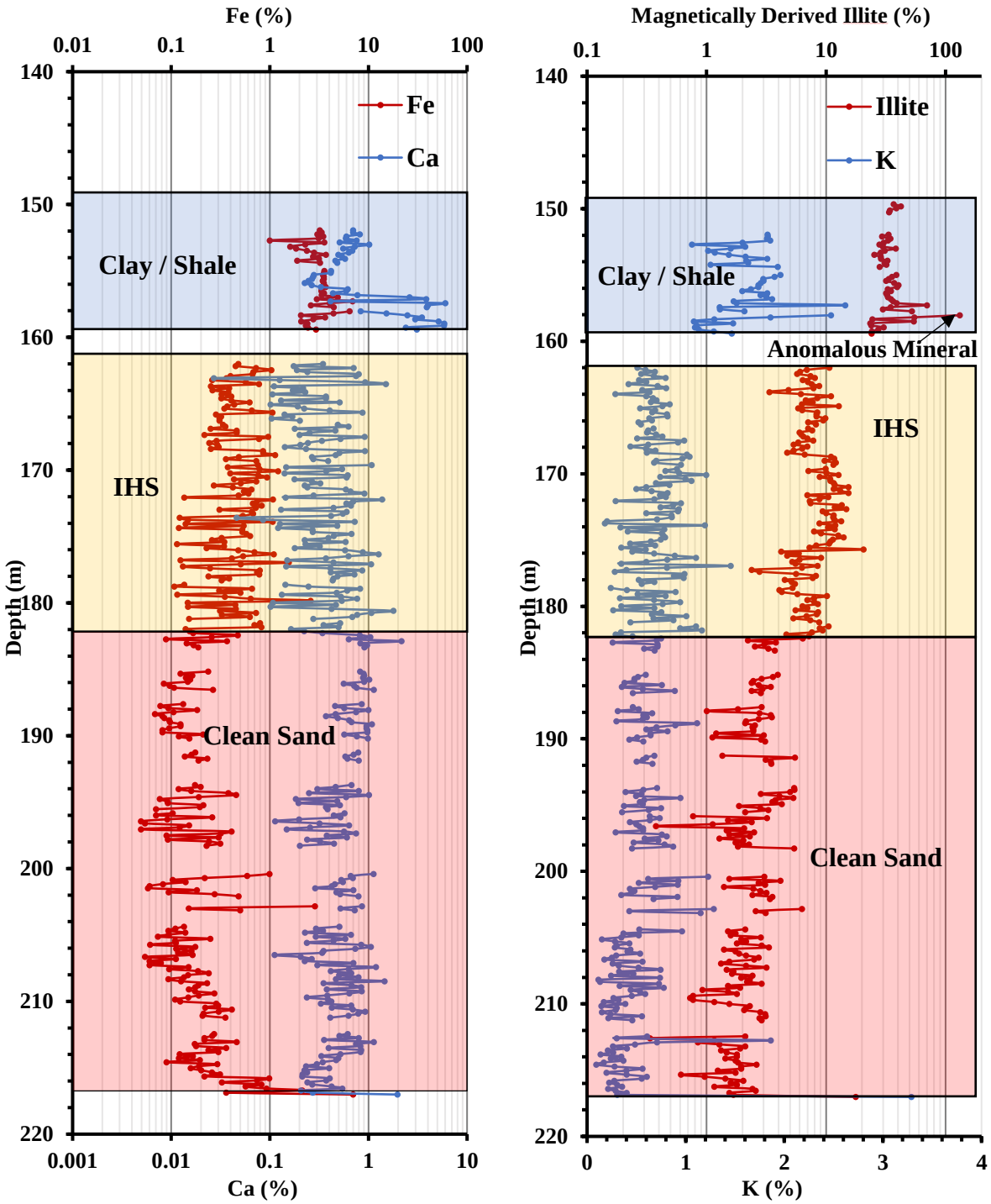

Fig. 14. X-ray fluorescence profiles with depth on the slabbed cores. **Left:** shows the iron (Fe) elemental contents from XRF (left curve), and the calcium (Ca) elemental contents from XRF (right curve). **Right:** shows the potassium (K) elemental contents from XRF (left curve) and for comparison the magnetically derived illite contents by volume (right curve).

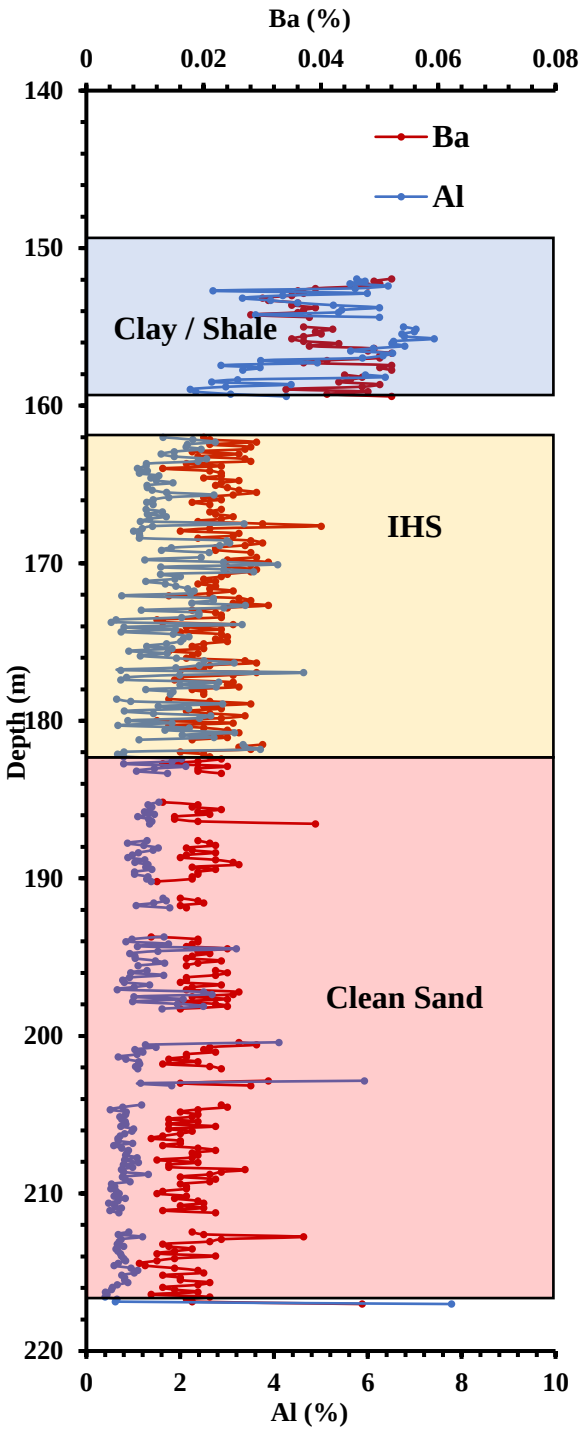

Fig. 15. X-ray fluorescence profiles with depth for the aluminium (Al) (left curve) and barium (Ba) elemental contents (right curve). Al is a component of illite, and Ba can be used to identify naturally cemented barite zones and/or drilling mud invasion.

3.4 Test for small remanence carrying particles

Reservoir samples often contain small particles of remanence carrying minerals [8, 9], such as the ferrimagnetic iron oxide magnetite, Fe_3O_4, or the canted antiferromagnetic mineral hematite, α-Fe_2O_3. These minerals have high magnetic susceptibility compared to paramagnetic clay minerals, and thus a small amount of them can sometimes affect the total susceptibility signal and cause an overestimate of the paramagnetic illite clay content if they are not accounted for. The presence of these remanence carrying particles can be identified from magnetic hysteresis curves by exhibiting loops or kinks at low fields [8, 9]. However, a quicker and simpler method to test for the presence of these particles is to see whether they acquire a magnetic remanence when subjected to a magnetic field. Acquisition of isothermal remanent magnetization (IRM) provides an ideal technique [10], since it is rapid, and produces the largest signal of any magnetic remanence method. A relatively high clay content IHS bed sample was subjected to stepwise direct field (DF) treatment in a Molspin pulse magnetizer. The sample acquired a small IRM, and the shape of the acquisition curve (which was close to saturation at an applied field of 130 mT) indicated that the remanence carrying particles were very likely magnetite. The acquisition curve was similar to 4.4-7.6 µm particle size magnetite [11] and represented an extremely small percentage of the total mass of the sample (0.0007 %). The magnetically derived illite content for this sample is 32.97% if one ignores the effect of this small amount of magnetite, and 30.67% illite if one corrects for the effect of the magnetite. Therefore the magnetite does not have a major effect on the illite determinations for this sample.

4 Conclusions

The following overall conclusions can be drawn:

1. Low field probe volume magnetic susceptibility profiles, which can be generated rapidly and non-destructively on this unconsolidated slabbed core, could clearly distinguish the 3 main lithologies in this oil sands well. Negative and close to zero volume magnetic susceptibility values indicated clean sand intervals, small positive values (generally up to about 5 x 10^{-5} SI) corresponded to inclined heterolithic stratification (IHS) beds or muddy sands, and higher positive values (generally greater than 10 x 10^{-5} SI) corresponded to shale. Whilst there were general correspondences between the magnetic results and the downhole log data for total gamma ray (GR) and spontaneous potential (SP), the magnetic results were better at distinguishing the 3 main lithologies.

2. The probe magnetic technique was particularly useful for distinguishing different lithologies, and quantifying variations in mineralogy, in this bitumen saturated core. This is a major advantage of the probe magnetic technique in oil sands core. Visual observations alone are often not able to distinguish the different lithologies or quantify the variations in mineralogy, since the black reservoir hydrocarbons obscure the visual details.

3. The raw probe magnetic susceptibility results were processed using a simple model mineral mixture of quartz + illite to derive illite contents. The

magnetically derived illite content was a useful parameter that distinguished the main lithologies, and exhibited good correlations with the following:
(i) *Total downhole gamma ray (GR) and spectral potassium gamma ray log data*.
(ii) *Downhole spontaneous potential (SP).* Permeable zones were indicated by low values of magnetically derived illite and large deflections to the left by the SP tool. However, the magnitude and direction of the deflection of the SP log depends on the difference in salinity between the formation water and drilling mud filtrate and would not show a deflection at a permeable zone if the salinities of the two fluids are equal. In contrast, the magnetic technique has the advantage that it can potentially identify a permeable zone in this situation regardless of whether the two salinities are equal or not.
(iii) *Fluid permeability.* A strong correlation was observed between the magnetically derived illite contents and core permeability values. The results were significantly better than the correlation between the core permeability and the SP log data.
(iv) *X-ray fluorescence (XRF).* Strong correlations between the magnetically derived illite contents and elemental contents of Fe, K and Al (all components of illite) supported the suggestion that illite was a major paramagnetic clay in the well.

4. The magnetically derived illite contents enabled one to identify thin layers of anomalous minerals, where "illite" contents were greater than 100% from the simple model. The total GR, spectral GR and SP logs did not generally identify these thin layers of anomalous minerals. The raw high resolution magnetic results were averaged over the same vertical interval as each wireline log data point averages, and therefore anomalous mineral identification from magnetic susceptibility was not merely due to resolution differences between the laboratory magnetic probe and the wireline tools.

5. Crossplots of magnetically derived illite content against XRF (elemental contents of Fe, K and Al) identified 3 clusters of points representing the 3 main lithologies (clean sand, IHS beds and shale), thus showing the potential of the combination of magnetic susceptibility and XRF measurements in the laboratory.

Cenovus FCCL Ltd are thanked for access to the slabbed core, downhole log and core permeability data, and a research grant to D. K. P. Matthias Halisch and Stefano Pruno are thanked for their thorough and constructive reviews of the manuscript.

5 List of abbreviations

DF	Direct Field
GR	Gamma Ray
IHS	Inclined Heterolithic Stratification
IRM	Isothermal Remanent Magnetization
SP	Spontaneous Potential
XRF	X-Ray Fluorescence

6 References

1. B. C. Agbo and D. K. Potter. Novel high resolution probe magnetic susceptibility and comparison with wireline gamma ray and grain size in an Albertan oil sand well. *Society of Exploration Geophysicists (SEG) Technical Program Expanded Abstracts 2014*: pp. 2590-2594. DOI: 10.1190/segam2014-1140.1 (2014).
2. T. H. To, D. K. Potter, A. Abiola, and V. T. Ebufegha. Probe magnetics as a rapid, non-destructive screening tool for consolidated and unconsolidated core in conventional and unconventional reservoirs. *Proceedings of the 2018 International Symposium of the Society of Core Analysts, 27-30 August 2018, Trondheim, Norway. Paper SCA 2018-057* (2018).
3. M. J. Ranger and M. K. Gingras, M. K. Geology of the Athabasca oil sands – field guide and overview. *Canadian Society of Petroleum Geologists*, Calgary, pp. 123 (2003).
4. D. K. Potter, P. W. M. Corbett, S. A. Barclay and R. S. Haszeldine, R. S. Quantification of illite content in sedimentary rocks using magnetic susceptibility—a rapid complement or alternative to X-ray diffraction. Journal of Sedimentary Research, Research Methods Papers Section, **74** (no. 5), 730-735 (2004).
5. D. K. Potter. Magnetic susceptibility as a rapid, non-destructive technique for improved petrophysical parameter prediction. Petrophysics, **48** issue 3), 191-201 (2007).
6. O. P. Ivakhnenko and D. K. Potter. Magnetic susceptibility of petroleum reservoir fluids. Physics and Chemistry of the Earth, **29**, 899-907 (2004).
7. B. Backman, K. Lindqvist, K. and E. Hyvönen. Manual for measuring soil samples with the Niton XL3 GOLDD+ XRF-instrument. Geologian Tutkimuskeskus, pp. 14 (2016).
8. O. P. Ivakhnenko and D. K. Potter. The use of magnetic hysteresis and remanence measurements for rapidly and non-destructively characterizing reservoir rocks and fluids. Petrophysics, **49**, (issue 1), 47-56 (2008).
9. A. Ali and D. K. Potter. Temperature dependence of the magnetic properties of reservoir rocks and minerals and implications for in situ borehole predictions of petrophysical parameters. Geophysics, **77** (no.3), 211-221 (2012).
10. D. Heslop, M. J. Dekkers, P. P. Kruiver and I. H. M. van Oorschot. Analysis of isothermal remanent magnetization acquisition curves using the expectation-maximization algorithm. Geophysical Journal International, **148** (1), 58-64 (2002).
11. D. K. Potter and A. Stephenson. Field-impressed anisotropies of magnetic susceptibility and remanence in minerals. Journal of Geophysical Research - Solid Earth, **95**, 15573-15588 (1990).